*J. Fluid Mech.* (1993), *vol.* 252, *pp.* 279–300



# A vertical buoyant jet with high momentum in a long ventilated tunnel

By S. J. BARNETT

Department of Applied Mathematics and Theoretical Physics, University of Cambridge, Silver Street, Cambridge CB3 9EW, UK

(Received 11 November 1992 and in revised form 20 January 1993)

In this paper the flow resulting from the release of buoyant material within a long tunnel is investigated. The source fluid is discharged through a nozzle of small radius with sufficiently high flow rate to ensure that the axial lengthscale of the buoyant jet (subsequently called the 'jet-length') is several times the depth of the tunnel, $d$. The ends of the tunnel may be either open or closed and a number of ventilation points may exist along it. Consideration of a source with high momentum is an important development in confined jet flow models, as most previous models have assumed that the source has little or no initial momentum. It is found that circulation cells are driven near to the source and that the concentration within them increases to a steady-state maximum. At a distance of about $2.5d$ from the source the buoyancy forces are then sufficiently strong to drive a two-layered stratified counterflow. The steady-state conservation equations are analysed in order to calculate the mean flow variables. The flow past a ventilation point and the characteristics of the secondary outflow are derived, enabling the calculation of the total number of vents needed to vent the buoyant layer. The time dependence of the mean concentration in the circulation cell near to the source is also deduced. This could be used to calculate time-dependent solutions for the other mean flow variables. All of the theoretical results are compared with experimental measurements.

## 1. Introduction

Jirka & Harleman (1979) have investigated the stability and mixing of a vertical planar buoyant jet discharged in a long channel of rectangular cross-section, filled with a shallow layer of water with a free surface. They observed that a source of momentum gave rise to circulation cells which extended over the full height of the channel (see figure 1). Up to two circulation cells on each side of the source were observed experimentally (in the planar case). Their experiments showed that the horizontal length of the primary cell can be estimated to be approximately $2d$, with the centre of the primary (first) circulation cell approximately $1.5d$ from the source axis and $0.5d$ from the tank base. Using a circular source, assuming that the width $\omega$ of the channel is of a similar order to the depth $d$, then circulations will be inhibited in the $(y, z)$-plane.

If the source is strongly buoyant, the buoyancy forces are sufficiently strong to inhibit the formation of a circulation cell and the jet spreads horizontally after impingement (see figure 2*a*). All the entrainment into the flow takes place into the buoyant jet before it has impinged and is thus independent of the outflowing layer.

A buoyant jet is characterized by its initial specific momentum and buoyancy fluxes $M_0$ and $B_0$ defined by

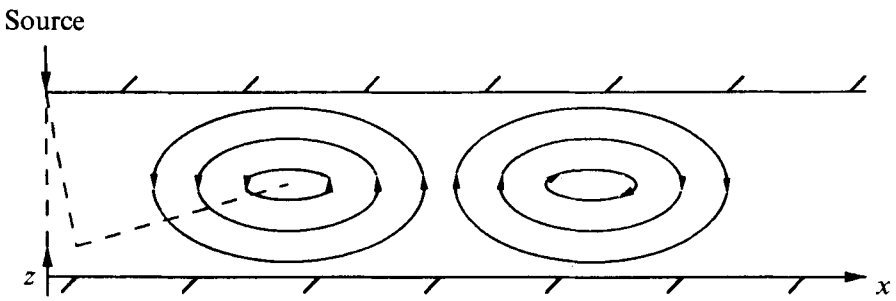


FIGURE 1. A schematic diagram of the flow produced by a lane non-buoyant discharge in a tunnel.

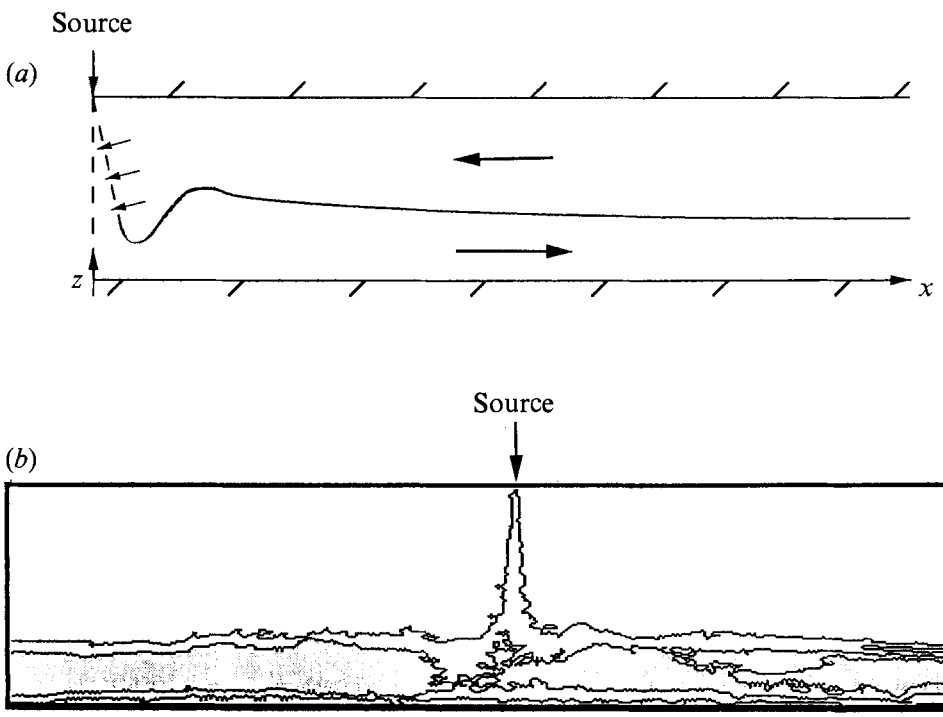


FIGURE 2. The flow produced by a strongly buoyant discharge into a tunnel; (*a*) a schematic diagram, and (*b*) an image taken from an experiment (in which dyed buoyant fluid was released from a circular nozzle in a Perspex tunnel). The image was obtained by digital analysis of a video of the flow – the lines are contours of equal mean concentration (averaged through the tank).

$$M_0 = \frac{1}{\pi}\int u_0^2 \,\mathrm{d}S, \quad B_0 = \frac{1}{\pi}\int u_0^2 g\frac{\Delta\rho}{\rho_a}\,\mathrm{d}S, \tag{1.1}$$

where $u_0$ denotes the velocity at the source fluid, which has density $\rho_0$; $\rho_a$ is a reference density; and $\Delta\rho = \rho_0 - \rho_a$. A lengthscale may be formed using these fluxes, called the 'jet-length' scale, $L_j$ (see, for example, Turner 1973), where

$$L_j = M_0^{\frac{3}{4}}/B_0^{\frac{1}{2}}, \tag{1.2}$$

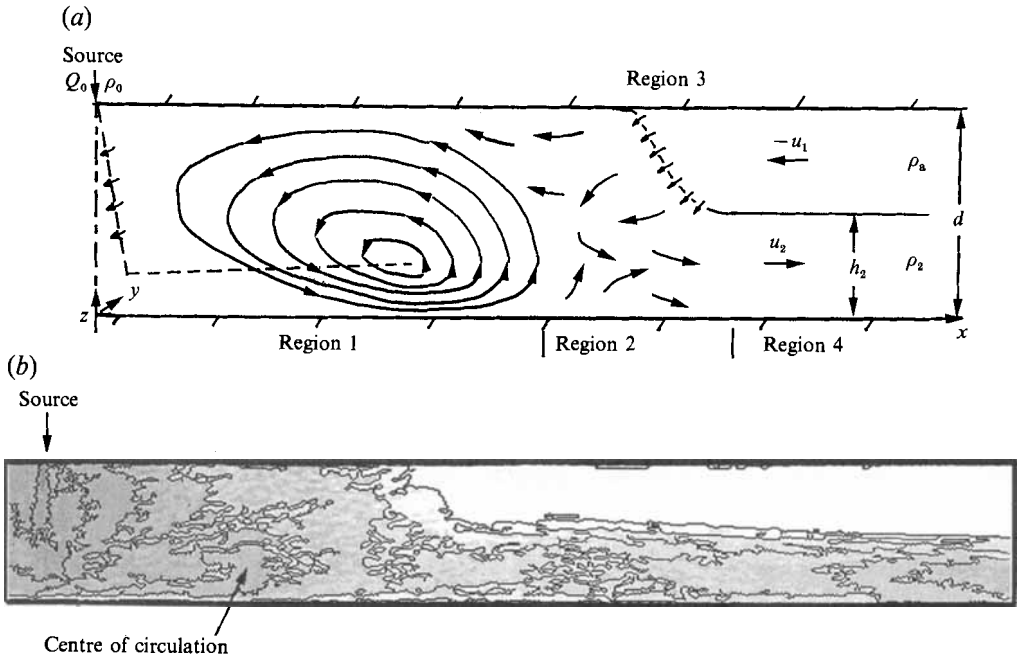


FIGURE 3. The flow produced by a buoyant source with high momentum; (*a*) schematic diagram, and (*b*) an image showing contours of dye concentration taken from an experiment).

which gives a measure of the lengthscale over which momentum forces will dominate buoyancy forces. In the situation considered here, $L_j$ is several times the depth $d$, and so the effects of buoyancy are negligible before impingement.

The resulting flow, drawn schematically in figure 3(*a*), is a combination of the above two extreme cases. The buoyant jet, discharged vertically and driven mainly by its initial momentum, spreads out horizontally on impingement. The jet velocities are sufficiently high to drive a circulation cell near to the source (region 1) which is observed to be well mixed, with the concentration increasing to a steady-state maximum. This increase in concentration is due to the re-entrainment of buoyant fluid into the jet itself. The centre of the circulation is approximately $1.5d$ from the source axis, but due to the buoyancy of the source the centre is less than $0.5d$ from the impingement boundary. The buoyancy of the jet is sufficient to inhibit the formation of a secondary circulation cell, which was observed in the non-buoyant (planar) case above, but turbulent momentum transfer excites the fluid on the outer boundary of the primary cell (region 2), entraining ambient fluid and releasing buoyant fluid (region 3) to the two-layer counterflow. The released fluid (from region 3) then flows horizontally in a stable buoyant layer with negligible entrainment cross the interface (region 4). A typical 'freeze-frame' of the flow is given in figure 3(*b*), demonstrating all of the features mentioned above. This flow has been observed previously by Lee (1980) and Andreopoulos, Praturi & Rodi (1986) in experiments with vertical buoyant jets in shallow water, although they merely consider the flow as an 'instability' of the 'stable' buoyancy-dominated flow.

This study has the obvious practical application to the modelling of a leak of natural (or other buoyant) gas within a tunnel or duct. Piped gas is often under high pressure and on escaping through a small hole, caused by corrosion, the flow described in this paper could be set up. Clearly it would be advantageous to know under what

circumstances the concentration levels of gas would pass required safety limits, and what configurations of vents would be most effective in venting the gas. Therefore, in this investigation the build-up of concentration within the tunnel and the dependence of the flow of buoyant fluid along it on the position, size and number of ventilation points is of particular importance. A further objective is the study of the concentration build-up within the primary cell and the effect of a ventilation point within it.

## 2. Analysis

In the following analysis it is initially assumed that the ventilation points are situated symmetrically on either side of the source, which is assumed to be negatively buoyant for ease of comparison with the experiments. Theoretically then, the flow should be symmetric about the source and so only one half is considered. Initially it is assumed that all the ventilation points are outside regions 1 and 2, and that there are sufficient vents to make no restriction on the inflow or outflow rates.

### 2.1. *Region 4: the stratified counterflow*

The two-dimensional flow of a buoyant layer has been previously studied by Ellison & Turner (1959), Wilkinson & Wood (1971) and Jirka & Harleman (1979), but only when the depth of the layer is small compared with the total depth and one layer has a free surface. The counterflow will now be re-examined when both layers are bounded by solid boundaries and the buoyant layer may have large depth.

The following assumptions are made in analysing the flow:

(i) the flow has reached a steady-state equilibrium;

(ii) the flow is mainly two-dimensional with vertical velocities sufficiently small for the flow to be considered horizontal with a hydrostatic pressure distribution;

(iii) there is negligible entrainment across the interface; Ellison & Turner (1959) gave a lower limit on the Richardson number

$$Ri = \frac{g\Delta\rho d}{\rho_a(\Delta u)^2}, \tag{2.1}$$

where $\rho_a$ is the ambient density and $\Delta u$ is the horizontal velocity shear: for entrainment across such an interface to be considered negligible, $Ri \approx 0.8$ (this limit is generally satisfied in the experiments);

(iv) the flow force is constant along region 4 (see Benjamin 1968);

(v) at large distances from the tunnel the environmental fluid is still and of uniform density.

Let the height of the lower layer be $h_2(x, t)$, with density $\rho_2(t)$ (independent of $x$ from (iii)) with mean velocity $u_2(x, t)$. The upper layer of inflowing ambient fluid has mean velocity $u_1(x, t)$ and depth $h_1(x, t) = d - h_2(x, t)$.

Assuming a hydrostatic pressure distribution $p(x, z) = p_1 - \rho g(z - h_2)$, where $p_1$ is the pressure at the interface, then the equations of horizontal motion for the upper and lower layers are

$$\frac{\partial h_1}{\partial t} + \frac{\partial}{\partial x}(u_1 h_1) = 0, \tag{2.2}$$

$$\frac{\partial h_2}{\partial t} + \frac{\partial}{\partial x}(u_2 h_2) = 0, \tag{2.3}$$

$$\frac{\partial u_1}{\partial t}+u_1\frac{\partial u_1}{\partial x}=-\frac{1}{\rho_a}\frac{\partial p_I}{\partial x}-g\frac{\partial h_2}{\partial x}-\frac{\partial}{\partial x}(\overline{u'^2})-\frac{\partial}{\partial y}(\overline{u'v'})-\frac{\partial}{\partial z}(\overline{u'w'}), \tag{2.4}$$

$$\frac{\partial u_2}{\partial t}+u_2\frac{\partial u_2}{\partial x}=-\frac{1}{\rho_2}\frac{\partial p_I}{\partial x}-g\frac{\partial h_2}{\partial x}-\frac{\partial}{\partial x}(\overline{u'^2})-\frac{\partial}{\partial y}(\overline{u'v'})-\frac{\partial}{\partial z}(\overline{u'w'}), \tag{2.5}$$

where $\overline{u'^2}$ etc. are the shear stresses associated with the turbulent fluctuating velocities $u'$, $v'$, $w'$ in the $x$-, $y$- an $z$-directions respectively. Equations (2.2) and (2.3) are equations of volume conservation, and can be obtained by integrating the continuity equation over $z$.

2.1.1. *Negligible shear stresses*

In the following analysis, the steady state is considered initially, and as a first approximation it is assumed that the shear stresses are negligible. (It may be shown, Barnett 1991, that the effect of the shear stresses is to cause a small variation in the depth of the buoyant layer, which is observed to be negligible in the present experiments.)

The equations then reduce to (substituting for $h_1(x)$)

$$\frac{\mathrm{d}}{\mathrm{d}x}(u_1(d-h_2))=0, \tag{2.6}$$

$$\frac{\mathrm{d}}{\mathrm{d}x}(u_2h_2)=0, \tag{2.7}$$

$$\frac{\mathrm{d}}{\mathrm{d}x}\left(\frac{u_1^2}{2}+\frac{p_I}{\rho_a}+gh_2\right)=0, \tag{2.8}$$

$$\frac{\mathrm{d}}{\mathrm{d}x}\left(\frac{u_2^2}{2}+\frac{p_I}{\rho_2}+gh_2\right)=0. \tag{2.9}$$

Integration of (2.7) and (2.6) with respect to $x$ gives

$$Q_2=\omega h_2(x)\,u_2(x), \tag{2.10}$$

where $Q_2$ is the constant volume flux of the lower layer, and

$$Q_1=\omega(d-h_2(x))\,u_1(x), \tag{2.11}$$

where $Q_1$ is the constant (negative) volume flux of the upper layer (of density $\rho_a$).

Thus in the steady-state, the equations of total volume and mass conservation over any vertical cross-section in the counterflow become

$$\tfrac{1}{2}Q_0=\omega(u_2h_2+u_1(d-h_2))=Q_2+Q_1, \tag{2.12}$$

and

$$\tfrac{1}{2}Q_0\rho_0=\omega(u_2\rho_2h_2+u_1\rho_a(d-h_2)) \quad \text{or} \quad \tfrac{1}{2}Q_0g_0'=Q_2g_2', \tag{2.13}$$

where $g_2'=((\rho_2-\rho_a)/\rho_a)g$ is the reduced gravity of the buoyant layer.

The interface pressure can be eliminated from (2.8) and (2.9) giving

$$\frac{\mathrm{d}}{\mathrm{d}x}\left(\frac{u_1^2}{2}-\frac{\rho_2}{\rho_a}\frac{u_2^2}{2}-g_2'h_2\right)=0, \tag{2.14}$$

and expanding this with the use of (2.10) and (2.11) gives

$$\left(\frac{u_1^2}{d-h_2}+\frac{\rho_2}{\rho_a}\frac{u_2^2}{h_2}-g_2'\right)\frac{\mathrm{d}h_2}{\mathrm{d}x}=0. \tag{2.15}$$

This means that $h_2$, and consequently $u_2$ and $u_1$ must have constant values over the outflow region.

(The alternative is that

$$\frac{u_1^2}{d-h_2}+\frac{\rho_2}{\rho_a}\frac{u_2^2}{h_2}-g_2'=0.$$

In the Boussinesq limit this reduces to the critical Froude number condition

$$F_1^2+F_2^2=1, \quad \text{where} \quad F_1^2=\frac{u_1^2}{g_2'(d-h_2)} \quad \text{and} \quad F_2^2=\frac{u_2^2}{g_2'h_2},$$

which corresponds to a jump in $h_2$. A jump is not observed experimentally (generally to obtain such jumps a controlling geometry, e.g. a ridge, is needed) and so this possibility is ignored.)

Hence the flow is governed by the three equations

$$\omega u_2 h_2 = Q_2, \tag{2.16}$$

$$Q_0 g_0' = 2Q_2 g_2', \tag{2.17}$$

$$u_1 = \frac{Q_0-2Q_2}{2\omega(d-h_2)}, \tag{2.18}$$

in the five unknowns $u_1$, $u_2$, $h_2$, $g_2'$ and $Q_2$. A further two conditions must be obtained from the near-field and far-field conditions.

2.1.2. *Balance of flow forces over the head*

The integral budget of momentum and pressure is constant in the entire domain. Benjamin (1968) used this balance in the flow forces over the 'head' in his study of the flow over an air pocket. He defined the 'flow force' $F$ as the sum of the horizontal momentum flux and the pressure forces. Thus if $\Delta\rho$ is the density variation from $\rho_a$

$$F=\int_0^\omega\int_0^d(\rho_a+\Delta\rho)\,u^2\,\mathrm{d}z\,\mathrm{d}y+\int_0^\omega\int_0^d\int_z^d(\rho_a+\Delta\rho)\,g\,dz'\,\mathrm{d}z\,\mathrm{d}y, \tag{2.19}$$

which, for the two-layered system above reduces to

$$\frac{F}{\omega\rho_a}=\frac{\rho_2}{\rho_a}u_2^2h_2+u_1^2(d-h_2)+\frac{p_I}{\rho_a}d-\tfrac{1}{2}gd^2+dh_2g+\tfrac{1}{2}h_2^2g_2'. \tag{2.20}$$

Benjamin's analysis may be extended to the current situation. Consider the flow over the head of the outflowing layer (assuming that it has not met a ventilation hole) in a frame moving with the outflowing layer (see figure 4*a*).

The incoming ambient fluid has speed $U$ and the speed of the fluid over the head is $u_*$ with $u_*=u_1-u_2$. The point O is a stagnation point, with pressure $p_O$.

Use of conservation of volume and the Bernoulli theorem along OA gives the flow force per unit width of the incoming fluid

$$F_{in}=p_O\,d+\tfrac{1}{2}\rho_a\,dU^2-\tfrac{1}{2}g\rho_a\,d^2. \tag{2.21}$$

Applying the Bernoulli theorem along OI, using the Bernoulli theorem to show that $p_B=p_O$ and $p_B=p_I+g\rho_2h_2$ gives

$$g\rho_2h_2=\tfrac{1}{2}\rho_a u_*^2+g\rho_a h_2, \tag{2.22}$$

or

$$u_*^2=2h_2g_2'. \tag{2.23}$$

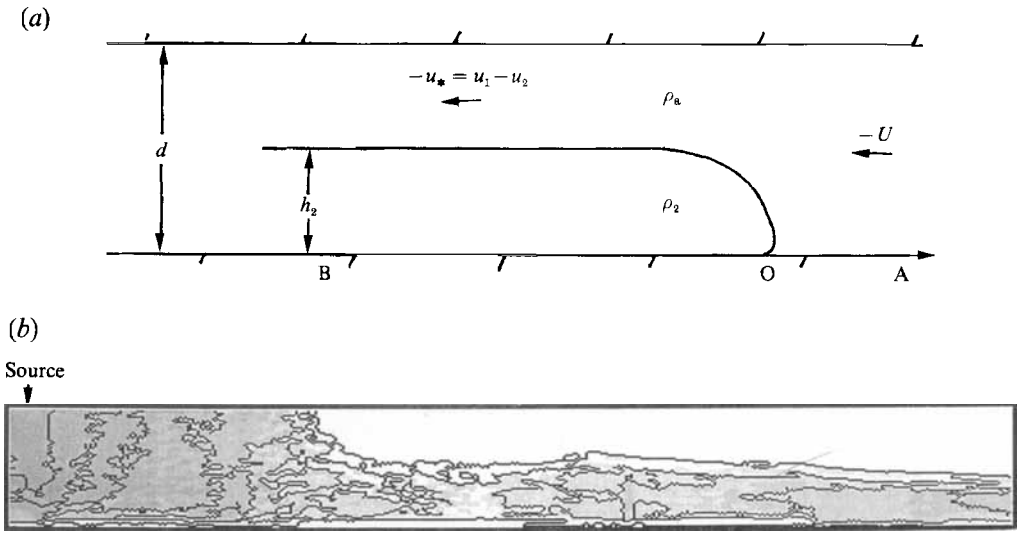


FIGURE 4. (*a*) Schematic diagram of the flow over the 'head'; (*b*) a typical image taken from experiment showing that the outflowing buoyant layer occupies half the depth of the tunnel.

The flow force per unit width of the outgoing fluid may be calculated similarly, giving

$$F_{\text{out}} = \rho_a u_*^2 (d - h_2) + (p_O - \tfrac{1}{2} u_*^2 \rho_a) d - \tfrac{1}{2} g \rho_a (d^2 + h_2^2) + \tfrac{1}{2} g \rho_2 h_2^2. \tag{2.24}$$

Equating the flow forces and using (2.21) and (2.24) yields

$$\frac{h_2}{d}(d - h_2)^2 g_2' = 2(\tfrac{1}{2}d - h_2) h_2 g_2' + \tfrac{1}{2} g_2' h_2^2. \tag{2.25}$$

Hence ignoring the uninteresting possibility of $g_2' = 0$, equation (2.25) gives two solutions for $h_2$: $h_2 = 0$ and

$$h_2 = \tfrac{1}{2}d, \tag{2.26}$$

i.e. the buoyant layer occupies half the depth of the tunnel, which is analogous to the solution obtained by Benjamin (1968) in his application to the flow over an air pocket.

Whilst moving in a frame at the propagation velocity of the density current, the hydrostatic pressure assumption is exact. Moncrieff & So (1989) presented a theory that included the effect of vorticity in the density current on its far-field behaviour. The pressure in the density current is then not hydrostatic except in the far field where the flow is horizontal. By allowing the density current to have an inflow speed far from the head, they found that there is partial cancellation in the corrective terms to (2.23), and so the above solution is more accurate than might otherwise be expected.

The above analysis will only apply before the head has met a vent; however it is observed experimentally that the outflow (between the mixing region the vent) continues to maintain this half-tunnel depth even after the head has flowed through or over a vent (see for example, figure 4*b* which shows a typical flow).

### 2.1.3. *Implications for the flow*

Making the assumption that the previously obtained result (2.26) holds between the start of the counterflow region and the first ventilation point, then the flow variables, $Q_2$, $u_2$ and $g_2'$ may be calculated.

Eliminating $u_2$ and $Q_2$ from (2.16), (2.17) and (2.18), and substituting for $h_2$ and $u_1$ using (2.23), (2.26) and $u_* = u_1 - u_2$, gives an equation for $g_2'$:

$$dg_2' = \left(\frac{Q_0}{d\omega}\right)^2 \left(\frac{2g_0'}{g_2'} - 1\right)^2. \tag{2.27}$$

Writing $g_2'/g_0' = \gamma_2$ then (2.27) may be rewritten

$$\gamma_2^3 - \tfrac{1}{4}B^3(2-\gamma_2)^2 = 0, \tag{2.28}$$

where

$$B^3 = 4Q_0^2/d^3\omega^3 g_0'. \tag{2.29}$$

Equation (2.28) could be solved numerically, but a good approximation to the solution, for small $B$, is given by

$$\gamma_2 = B - \tfrac{1}{3}B^2. \tag{2.30}$$

The corresponding approximate solutions for $u_2$, $u_1$, $Q_2$ and $g_2$, including the term of order $B^2$ in (2.30), are

$$u_2 = \tfrac{1}{2}(dg_0')^{\frac{1}{2}} B^{\frac{1}{2}}(1 + \tfrac{1}{3}B) \approx \frac{1}{\sqrt{2}}(h_2 g_2')^{\frac{1}{2}}, \tag{2.31}$$

$$u_1 = -\tfrac{1}{2}(dg_0')^{\frac{1}{2}} B^{\frac{1}{2}}(1 - \tfrac{2}{3}B) \approx -\frac{1}{\sqrt{2}}(h_2 g_2')^{\frac{1}{2}}, \tag{2.32}$$

$$Q_2 = \frac{1}{2}\frac{Q_0}{B}(1 + \tfrac{1}{3}B), \tag{2.33}$$

$$g_2' = g_0' B(1 - \tfrac{1}{3}B). \tag{2.34}$$

Generally, $B$ is small and so the terms of order $B^2$ could be neglected. In this case, note also that the total volume flux of the outflowing buoyant layers, $2Q_2$, is considerably larger than that of the source. The reduced gravity of the buoyant outflow will be lower than that of the source by an equal factor (see (2.17)). Note also that the solution implies that the Richardson number has a value of approximately unity and is approximately independent of the source conditions. This would explain why negligible entrainment between the layers is observed in the experiments.

In the above solution, (2.31)–(2.34), it was assumed that the value of the parameter $B$ is small. This is generally the case (in the experiments described in §3, $B \ll 1$), but the behaviour of the solution to (2.28) for large $B$ may also be considered.

The value of $B$ may be increased (equivalent to increasing the flow rate or decreasing the reduced gravity of the source) and the value of the solution (2.28), $\gamma_2$, increases correspondingly. However when $B^3 = 4$ then the solution to (2.28) is $\gamma_2 = 1$, i.e. the reduced gravity of the buoyant outflow is equal to that of the source. In this case $Q_2 = \frac{1}{2}Q_0$, $u_2 = Q_0/\omega d$ and $u_1 = 0$. Thus when $B^3 = 4$ the solution implies that there is zero entrainment into the primary cell. This is clearly a physically unrealistic situation, as $B^3 = 4$ is equivalent to having an enormous value for the jet length ($B^3 = 4$ implies that $L_j \approx O(10^5)d$ with typical experimental values) and under such circumstances there would be considerable entrainment.

Increasing $B$ further yields $\gamma_2 > 1$, a physically impossible result. It must therefore be concluded that the model may be applied to situations in which $B \ll 1$. Physically this states that the volume flux of the buoyant layer is sufficiently small to be easily transported as a gravity current (i.e. the model is appropriate). For large values of $B$, it is expected that the source fluid will form a 'plug', driving the ambient fluid from the tunnel.

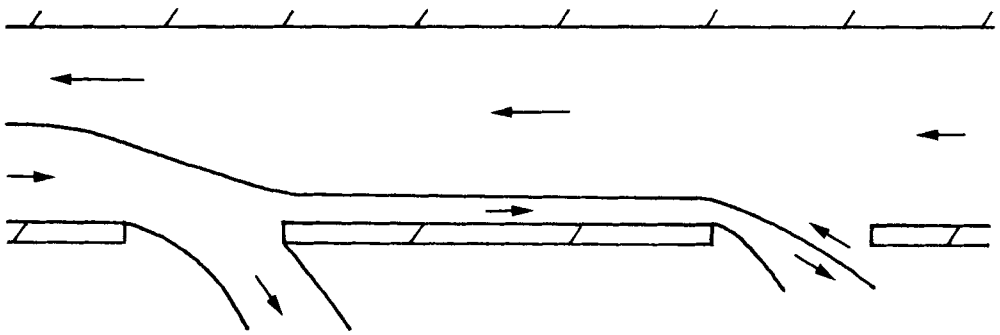

FIGURE 5. A schematic diagram of a typical flow with ventilation points.

2.1.4. *Flow with energy loss at the head*

The analysis may be extended to include the possibility of energy loss or supply. Equation (2.23) may be modified by including a head loss $\zeta$. The balance of flow forces is unaffected by the energy loss, and in this case the balance gives

$$u_*^2 = dg_2' \quad \text{and} \quad h_2 = \tfrac{1}{2}d+\zeta. \tag{2.35}$$

Hence a flow with $h_2 > \frac{1}{2}d$ is possible with an energy loss ($\zeta > 0$), and a flow with $h_2 < \frac{1}{2}d$ implies an energy supply to the counterflow ($\zeta < 0$). Equation (2.28) is modified to

$$\gamma_2^3 - \tfrac{1}{4}B'^3[2-\gamma_2(1+2\zeta/d)]^2 = 0, \quad \text{where} \quad B' = \left(\frac{4Q_0^2 d}{(d^2-4\zeta^2)^2\omega^2 g_0'}\right)^{\frac{1}{5}}. \tag{2.36}$$

Neglecting all but the largest terms, the modified approximate solutions are

$$\left.\begin{aligned} u_2 = \tfrac{1}{2}(dg_0')^{\frac{1}{2}}B'^{\frac{1}{2}}(1-2\zeta/d), \quad u_1 = -\tfrac{1}{2}(g_0' d)^{\frac{1}{2}}B'^{\frac{1}{2}}(1+2\zeta/d), \\ Q_2 = \tfrac{1}{2}Q_0/B', \quad g_2' = B'g_0'. \end{aligned}\right\} \tag{2.37}$$

Note that $B' \geqslant B$ for all $\zeta$ and, if the flow is not energy conserving, the flow rate $Q_2$ will be less than its value in (2.33) whereas the reduced gravity $g_2'$ will be greater than in (2.34).

## 2.2. *Counterflow with ventilation points*

A typical ventilation system is shown schematically in figure 5. The $N$ ventilation points have area $A_i$ ($i = 1 \ldots V$). Without the presence of a 'head' the analysis of §§2.1.2 and 2.1.3 cannot be used and so it is assumed here that the flow has pre-set initial values for the flow variables $h_2$ etc. In practice though, it is observed that the outflow maintains its initial depth of $\frac{1}{2}d+\zeta$ long after the fluid has flowed through a vent (or vents).

2.2.1 *The volume flux through the vent*

It has been shown (Linden, Lane-Serff & Smeed 1990) that the exchange flow $Q$ of a buoyant fluid through a hole in a closed box containing buoyant fluid takes the form

$$Q \approx kA(g'h)^{\frac{1}{2}}, \tag{2.38}$$

where $A$ is the area of the hole, $g'$ is the reduced gravity, $h$ is the depth of the buoyant fluid and $k$ is a constant dependent on the shape and orientation of the hole. For a

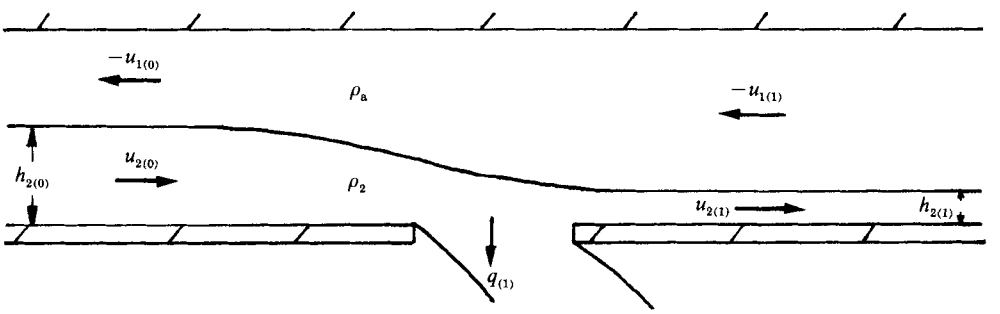


FIGURE 6. A schematic diagram of the flow over a vent.

square hole in vertical boundary the value of $k$ is approximately 0.25 with equal flow into and out of the hole. It is assumed that a similar relation holds in the present situation with the flow out of the first ventilation hole $q_{(1)}$ given by

$$q_{(1)} = k_1 A_1 (g_2' h_{2(0)})^{\frac{1}{2}}, \tag{2.39}$$

where $k_1$ is a constant and $h_{2(0)}$ denotes the initial value of $h_2$.

2.2.2. *The flow over the vent*

The flow over a ventilation hole is drawn schematically in figure 6. It is assumed that the fluid flow past the hole has height $h_{2(1)}$ and reduced gravity $g_2'$, i.e. that no mixing has taken place, and that the velocities of the lower and upper layers are $u_{2(1)}$ and $u_{1(1)}$ respectively.

Continuity of volume in the upper and lower layers then gives

$$\omega u_{1(0)}(d-h_{2(0)}) = \omega u_{1(1)}(d-h_{2(1)}), \tag{2.40}$$

$$\omega u_{2(0)} h_{2(0)} - q_{(1)} = \omega u_{2(1)} h_{2(1)}. \tag{2.41}$$

Equation (2.14) may also be applied, giving

$$(u_{1(0)}^2 - u_{1(1)}^2) - \frac{\rho_2}{\rho_a}(u_{2(0)}^2 - u_{2(1)}^2) - 2g_2'(h_{2(0)} - h_{2(1)}) = 0. \tag{2.42}$$

Hence $u_{1(1)}$ and $u_{2(1)}$ may be eliminated, giving an equation for $h_{2(1)}$:

$$u_{1(0)}^2\left[\left(\frac{d-h_{2(0)}}{d-h_{2(1)}}\right)^2 - 1\right] = \frac{\rho_2}{\rho_a}\left[\left(\frac{\omega u_{2(0)} h_{2(0)} - k_1 A_1 (g_2' h_{2(0)})^{\frac{1}{2}}}{\omega h_{2(1)}}\right)^2 - u_{2(0)}^2\right] - 2g_2'[h_{2(0)} - h_{2(1)}]. \tag{2.43}$$

The process above may then be repeated for subsequent vents until the maximum flow through a vent given by (2.39) is greater than the buoyant-layer volume flux approaching it (i.e. $q_{(i)} > Q_{2(i)}$). Thus repeated application of (2.43) represents a method by which the number of ventilation points required for total ventilation of the buoyant layer can be calculated.

Equation (2.43) may be rewritten making use of the solution obtained in §2.1.4, (2.37), for small $\zeta$ and the Boussinesq approximation, giving

$$\left[\frac{(1-4\zeta'^2)}{1-h_{2(1)}'}\right]^2 = \left[\frac{(1-4\zeta'^2) - 2\sqrt{2k_1 A_1'}(1+2\zeta')^{\frac{1}{2}}}{h_{2(1)}'}\right]^2 - 16[1-2h_{2(1)}'], \tag{2.44}$$

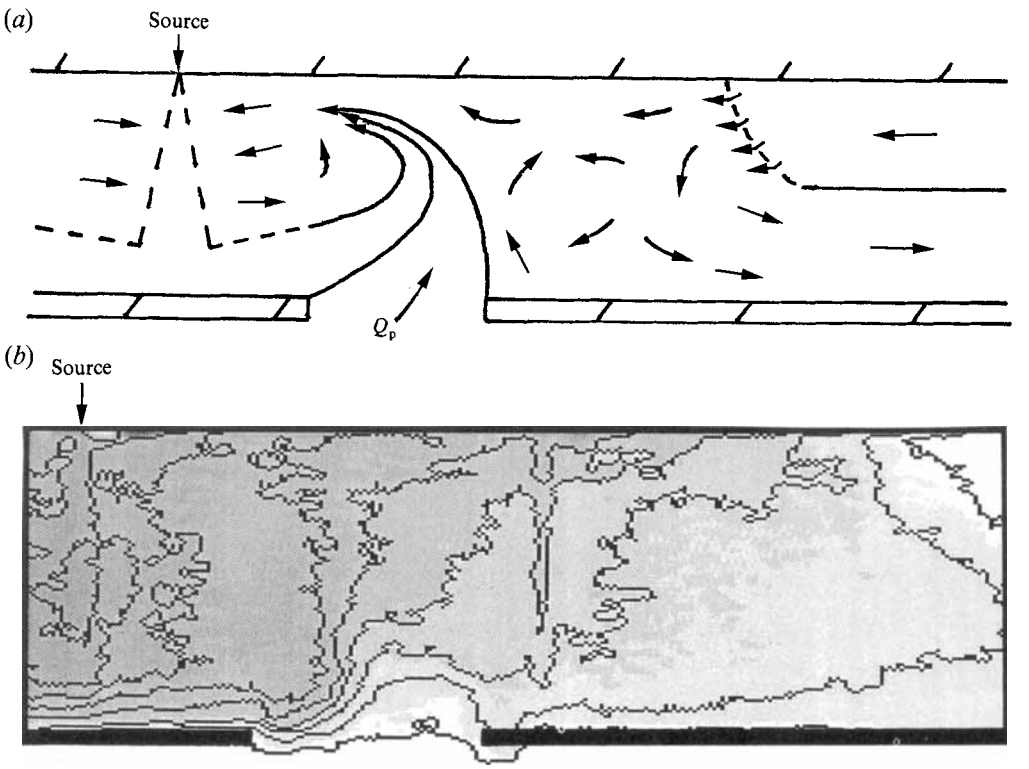


FIGURE 7. The flow with a vent in the primary cell; (*a*) a schematic diagram, and (*b*) an image taken from experiment.

where $$A_1' = A_1/\omega d, \quad h_{2(1)}' = h_{2(1)}/d, \quad \zeta' = \zeta/d. \tag{2.45}$$

This final equation shows that for a given inflow depth $h_{2(0)}$ (set by $\zeta'$), the secondary outflow height $h_{2(1)}$ is dependent (to first order in $B'$) only on the area of the opening. (Note that the secondary height is considered here rather than the secondary volume flux as it is easier to measure $h_{2(1)}$ in experiments.)

### 2.2.3. *A ventilation point in the primary cells*

It was mentioned earlier that a ventilation point in the primary cell region allows environmental fluid to be 'sucked' into the tunnel due to the drop in pressure associated with the circulation. This flow is drawn schematically in figure 7(*a*). Figure 7(*b*) is taken from experiment, the concentration contour lines clearly showing the flow through the vent close to the source. If the volume flux of the inflowing environmental fluid into the primary cell is $Q_p$, then the equations of conservation of volume and mass flux become

$$\tfrac{1}{2}Q_0 + Q_p = Q_1 + Q_2, \tag{2.46}$$

$$\tfrac{1}{2}Q_0 g_0' = Q_2 g_2'. \tag{2.47}$$

It is expected that the velocity of the inflowing fluid is proportional to the exit velocity of the source. Thus an expression for $Q_p$ may take the form

$$Q_p = k_p A_p \frac{M_0}{Q_0} f\left(\frac{x_p}{d}, \frac{g_c'}{g_0'}\right), \tag{2.48}$$

where $A_p$ is the area of the opening, $k_p$ is a constant, and $f(x_p/d, g_c'/g_0')$ is the functional dependence on the distance of the centre of the vent $x_p$ from the source axis and on the mean reduced gravity within the primary circulation cell, $g_c'$.

Because of the increased volume flux entering the primary cells, the volume flux of the outflow is expected to increase similarly.

Using the new conservation equations above it is possible to derive an equation analogous to (2.28), viz

$$\gamma_2^3 = \tfrac{1}{4}B'^3(2-P\gamma_2)^2, \quad \text{where} \quad P = (1+2Q_p/Q_0)(1+2\zeta'). \tag{2.49}$$

The value of $P \geqslant 1$ can be large which makes it hard to find a general approximate solution to (2.49) but a satisfactory approximation (a quadratic fit) is given by

$$\gamma_2 = B'[1-\tfrac{5}{16}PB'+\tfrac{2}{41}P^2B'^2+\ldots] \quad \text{for} \quad 0 \leqslant PB' \leqslant 2 \quad \text{with} \quad g_2' = \gamma_2 g_0'. \tag{2.50}$$

Of more significance to the problem of venting the buoyant fluid is the new value of the outflow rate. This is given by

$$Q_2 = \frac{Q_0}{2\gamma_2} \approx \frac{Q_0}{2B'}[1+\tfrac{5}{16}PB'+\ldots], \tag{2.51}$$

and the layer velocities are given by

$$u_2 = \tfrac{1}{2}(dg_0')^{\frac{1}{2}}B'^{\frac{1}{2}}(1-2\zeta')[1+\tfrac{5}{16}PB'+\ldots], \tag{2.52}$$

$$u_1 = -\tfrac{1}{2}(dg_0')^{\frac{1}{2}}B'^{\frac{1}{2}}(1+2\zeta')\left[1+\left(\frac{5}{16}-\frac{15}{16(1+2\zeta')}\right)PB'+\ldots\right]. \tag{2.53}$$

From these expressions it can be seen that the inflow $Q_p$ is not merely reflected in an equal increase in the outflow $Q_2$, but that $Q_2$ increases by approximately $5Q_p/16$ only (for large $Q_p$), with the inflowing velocity $u_1$ decreasing significantly to compensate. Thus the system is able to adjust to cope with relatively large volumes of environmental fluid being sucked into the primary cell, with quantitatively smaller changes to $Q_2, g_2'$ and $u_2$. The increase in $Q_2$, and the decrease in $g_2'$, may mean that a larger number of vents (than was the case without a vent in the primary cell region) are needed to vent the buoyant layer. This increase has been observed in experiments.

#### 2.2.4. *A ventilation point in region 2*

This case is probably the most complex problem resulting from ventilation because a vent in the mixing region 2 will allow fluid to flow both into and out of the tunnel. Initially there is little buoyancy of the fluid inside the tunnel and so environmental fluid may be sucked in by the circulating fluid in the primary cell. However with increasing time the buoyancy of the fluid inside the tunnel increases causing an increasing resistance to the outflow. Eventually the buoyancy forces may become larger than the suction forces and buoyant fluid will flow out of the ventilation point.

### 2.3. *The concentration build-up in the primary cell*

The concentration within the primary cell increases to a steady-state maximum, this increase being due to the re-entrainment of buoyant fluid into the jet and the eventual balance between the buoyancy forces of the mixed region and the opposing inertial and frictional forces of the counterflow system. The large 'jet length' of the source means that the source fluid and any inflowing environmental fluid are very rapidly mixed throughout the primary cell, and so it is appropriate to consider the mean reduced gravity $g_c'$ of the fluid within the primary cell, which is assumed to have length $l$.

Suppose the buoyant fluid layer has volume flux $Q_2(g_2')$. The equation for conservation of volume flux (2.12) will still apply, but the equation for conservation of mass (2.17) is modified to

$$\frac{\mathrm{d}g_c'}{\mathrm{d}t} = \frac{1}{l\omega d}(\tfrac{1}{2}Q_0 g_0' - Q_2(g_2')\, g_2'(t)), \tag{2.54}$$

and hence (2.17) is satisfied when $\mathrm{d}g_c'/\mathrm{d}t = 0$. This is the equation governing the concentration build-up within the primary cell, clearly dependent on the nature of the function $Q_2(g_c')$.

A first-order form for $Q_2(g_2')$ may be found by observing that (2.37) and (2.16) imply that

$$Q_2(g_2') \sim g_2'^{\frac{1}{2}}. \tag{2.55}$$

Writing

$$Q_2(g_2') = \tfrac{1}{2}Q_0 g_0' \beta g_2'^{\frac{1}{2}}, \tag{2.56}$$

for convenience, (2.54) then becomes

$$\frac{\mathrm{d}g_c'}{\mathrm{d}t} = \frac{Q_0 g_0'}{2l\omega d}(1 - \beta\kappa^{\frac{3}{2}} g_c'^{\frac{3}{2}}), \tag{2.57}$$

where it has been assumed that $g_2'(t) = \kappa g_c'(t)$ – the constant $\kappa \leqslant 1$ allows for the dilution of the mixed fluid in region 2 by the incoming ambient fluid. Also, assuming that in the limit $t \to \infty$ the value of $g_2'(t)$ tends to the steady-state solution given in §2.1, then the parameter $\beta$ may be found to be

$$\beta = \frac{\omega d^{\frac{3}{2}}(1 - 4\zeta'^2)}{2g_0' Q_0}[1 + (\tfrac{15}{32})\, PB' + \ldots], \tag{2.58}$$

recalling that $P = 1$ if there is no vent in the primary cell, and that $B'$ is small (as long as $\zeta'$ is small). With typical experimental values, $\beta \approx 0.4$. Equation (2.57) has solution

$$-\tfrac{1}{3}\ln\left(\frac{(1-\eta)^2}{1+\eta+\eta^2}\right) - \frac{2}{\sqrt{3}}\arctan\left(\frac{2\eta+1}{\sqrt{3}}\right) + \frac{2\pi}{6\sqrt{3}} = \frac{Q_0 g_0' \beta^{\frac{3}{2}}}{2l\omega d}t, \quad \text{where} \quad \eta = (\kappa^{\frac{3}{2}}\beta)^{\frac{1}{3}} g_c'^{\frac{1}{2}}, \tag{2.59}$$

which will be compared with experiment, measuring the mean primary cell concentration and the mean outflow concentration to compute $\kappa$. Equation (2.57) can be written in the form

$$\frac{\mathrm{d}\tilde{g}_c'}{\mathrm{d}t} = \kappa(1 - \tilde{g}_c'^{\frac{3}{2}}). \tag{2.60}$$

where

$$\tilde{g}_c' = (\beta^{\frac{3}{2}}\kappa) g_c' \quad \text{and} \quad \tilde{t} = \beta^{\frac{3}{2}}\frac{Q_0 g_0'}{2l\omega d}t. \tag{2.61}$$

Equations (2.60) and (2.61) are the form of (2.57) that will be used in the comparison with experimental data as it is easier to obtain $\tilde{g}_c'$ than $g_c'$ using digital video analysis. Note that the maximum value of $g_c'(t)$ is given by

$$g_c' = 1/\kappa\beta^{\frac{3}{2}}. \tag{2.62}$$

The time-dependent solution for $g_c'$, (2.59), and the corresponding solution for $g_2'$, (2.59), could be used to calculate time dependencies for all of the other flow variables

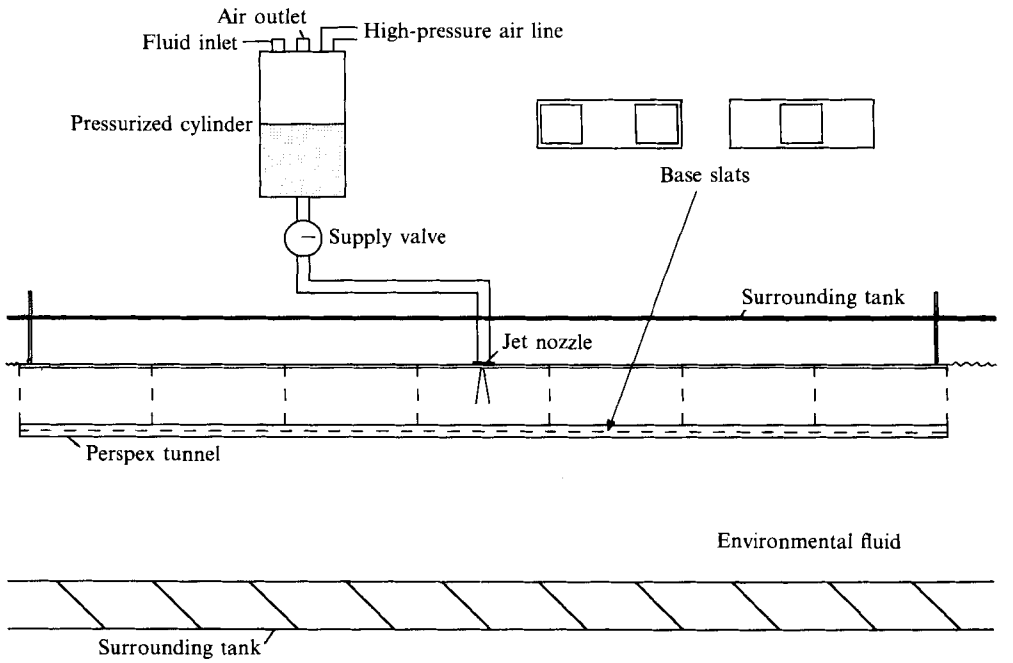


FIGURE 8. The experimental apparatus.

(by using (2.16) and (2.18)). However, it will be shown that the steady state is reached rapidly in practice and thus the steady-state solution, (2.31)–(2.34), is likely to be of greater use.

## 3. Experimental method

The experiments were carried out in a Perspex tunnel of width and depth 10 cm and length 210 cm (see figure 8). The base of the tunnel consisted of seven slats of length 30 cm in which there were either one or two ventilation holes of area 64 $cm^2$ in which stoppers could be placed. Vertical aluminium dividers could be used to vary the length of the tunnel, or to open or close the ends. Except when examining the effect of ventilation points, all the vents were closed and the ends of the tunnel were open. The Perspex tunnel was placed in a tank of length 9.4 m, depth 47 cm and width 26 cm. The tank was then filled with water until the surface was at the same height as the top of the tunnel. The water was allowed to settle for at least an hour before each experiment.

The outflow of buoyant fluid was represented by a solution of salt water. A small amount of dye (food colouring) was added to the salt solution and the flow visualized using the shadowgraph technique. The dyed salt solution was introduced into the tunnel using a fine circular nozzle of radius 0.25 mm supplied by a brass cylinder which was constantly connected to a high-pressure air supply, ensuring steady flow rates of up to 7.5 $cm^3\ s^{-1}$. Source reduced gravities of up to 65 cm $s^{-2}$ were used.

### 3.1. *Video analysis*

By recording the experiments on video tape, digital video analysis can be used to calculate mean source concentrations along lines perpendicular to the walls of the tunnel. This is a satisfactory way of measuring concentrations in this problem as the

flow is two-dimensional in the counterflow, and in the primary cell only mean values are needed for comparison with the theory.

The video picture is divided up into a grid of pixels each with an intensity (from 0, black, to 255, white) dependent on the dye concentration. Variations in the background illumination could be compensated for by removing an image of the initial state of the apparatus by division. An experiment was performed to investigate the variation of pixel intensity value with dye concentration. This experiment confirmed that the dye/intensity relationship is linear for sufficiently low dye concentrations. So by making one density measurement at a specific point in the flow from a fluid sample (for example using a Paar density meter) and comparing it to the intensity value there, it is easy to calculate the density/intensity relationship. Good consistency was found in all cases.

## 4. Results

Four sets of experiments were carried out. The experiments are described first, and then the theoretical predictions are compared with the observations.

### 4.1. *The flow and its dependence on the source flow rate*

Figure 9(*a–f*) shows the time development of a typical, unventilated run. Notice particularly the development of the gravity current, with the outflow occupying approximately half the depth of the tunnel.

In general, the flow was symmetric for symmetric configurations of vents and in such 'perfect' conditions, the outflow occupied approximately half the depth of the tunnel, in agreement with (2.26) (to $\pm 0.05d$). This type of situation appears to be somewhat unstable and occasionally the flow became permanently asymmetric, with the outflow on one side of the source occupying a much larger depth and the outflow on the other side occupying a lesser depth. These cases were in the minority however, and are thought to be the result of initial imbalances in the temperature between the ends of the tunnel, producing a slight bias on the flow within it. Under good conditions, then, the predictions for the bulk flow can be checked.

Experiments were carried out to test the dependence of $u_2$ and $g_2'$ on the source flow rate $Q_0$. The source flow was altered by changing the pressure in the brass chamber, the valve on which ensures constant pressure and hence constant flow rate. For each setting of the pressure, the flow was allowed to develop to a steady state before measurements were taken. The value of $g_0'$ was kept constant.

It was found that a minimum source flow rate was required to maintain the flow system of §2, i.e. the input of momentum below this threshold was insufficient to mix the fluid to the extent assumed in the analysis. At the threshold it was found that the ratio, $\delta$, of jet length to tunnel depth was

$$\delta = L_j/d = 2.9,$$

i.e. although $\delta > 1$ in all of the experiments, for the system to contain a well-mixed recirculating central region, $\delta \geqslant 2.9$ is required.

The outflow velocities were measured by injecting a small volume of green dye into the outflow and measuring the time taken for the dye patch to travel a distance of 30 cm along the tunnel. There was little mixing within the buoyant outflow and so the dispersion of the dye patch was minimal. The experimental results agreed well with the predictions for the steady-state bulk flow variables (for further details see Barnett 1991).

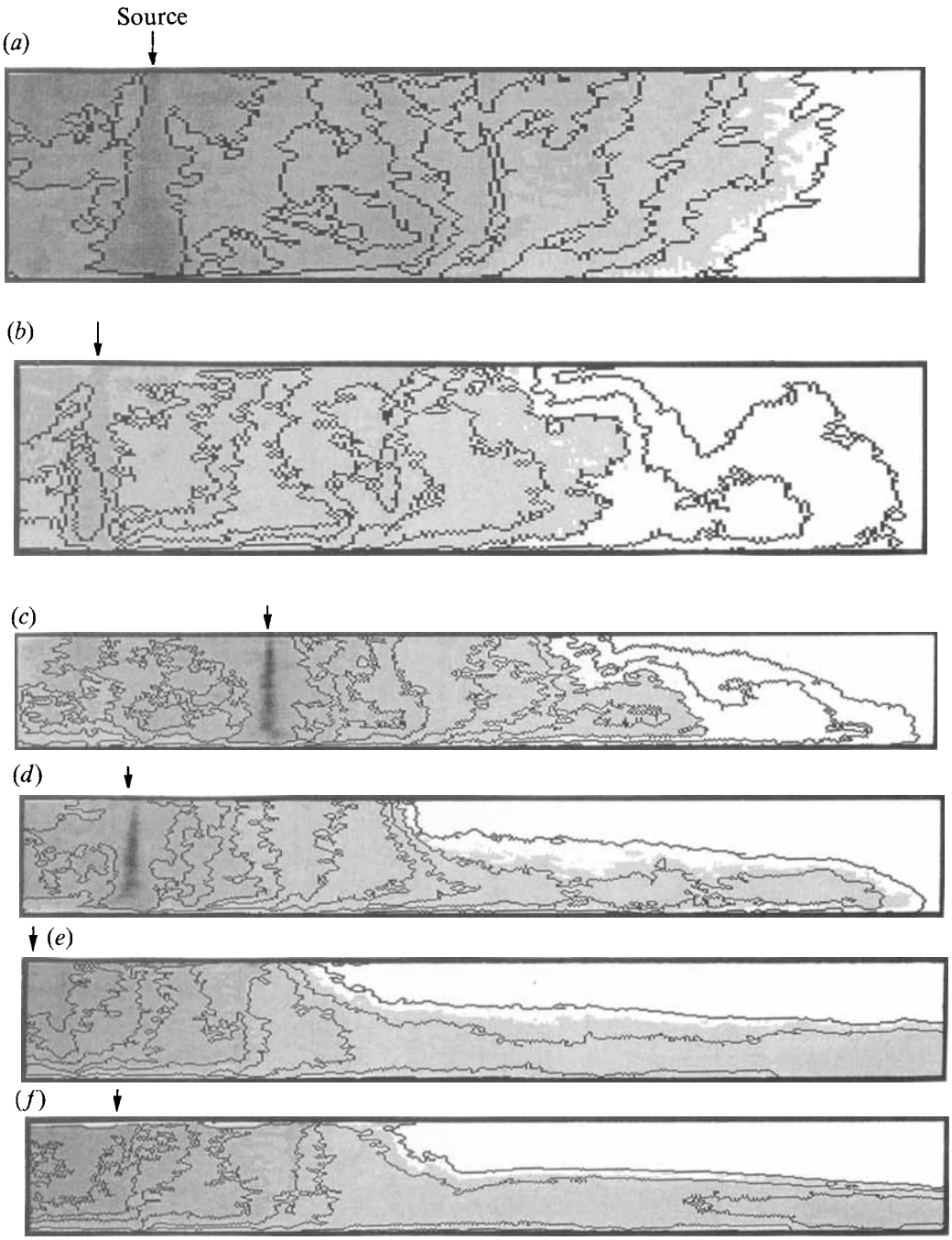


FIGURE 9. Images showing the development of the flow: (*a*) $t = 10$ s, (*b*) 20 s, (*c*) 30 s, (*d*) 40 s, (*e*) 50 s, (*f*) 100 s.

### 4.2. *The concentration in the primary cell*

To analyse the flow, frames were taken from the video every 10 s, the background removed, and the dye intensities calculated by digital analysis. The mean primary cell concentration was calculated by averaging the intensities over a section of the tunnel

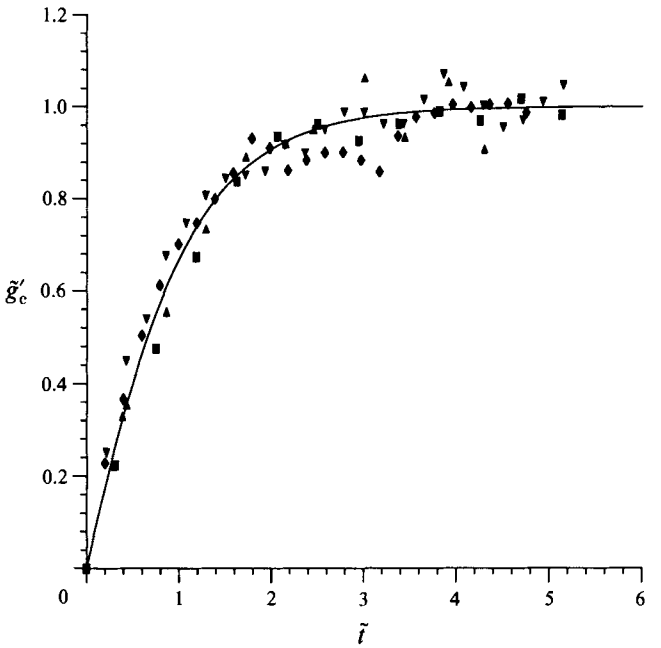


FIGURE 10. The time dependence of the primary cell concentration: comparison between the experimental data, and the theoretical curve of (2.60) with $\kappa = 0.9$.

of length $l = 2.5d$, with one edge on the axis of the source, the same section being used for each experiment. The data were put into the appropriate form and compared with equation (2.60).

The data and the solution to (2.60) with $\kappa = 0.9$ are plotted in figure 10. The agreement with the theoretical curve is excellent although there is some scatter about the equilibrium state, possibly due to fluctuations in the entrainment flow of the ambient layer into the primary cell. This choice of $\kappa$ is reasonable, agreeing with initial test measurements of $g'_2$ and $g'_c$ from which $\kappa$ may be calculated. The transition to equilibrium takes place over a relatively short time, usually within two minutes in these experiments.

### 4.3. *The flow over a vent*

The third objective of the experimental study was to measure the dependence of the secondary outflow height following flow over a vent in the counterflow region, on the area of the vent.

The source was switched on and the flow allowed to reach equilibrium. A large vent far from the source was then made by sliding one of the base slats along to make a vent of sufficiently large area for all the outflow to be easily vented by this single hole.

The vent was then closed by slowly pushing the slat back to its original position in small steps, recording the secondary outflow height at each stage. Of particular importance is the minimum size of hole required to vent all the fluid – this will enable the calculation of the constant $k$ in (2.44). In practice the measurement of $h_{2(1)}$ proved difficult due to the presence of a layer of mixed fluid between the outflowing layer and the inflowing environmental fluid. Hence the secondary outflow height measured was that of moving fluid only.

The data are plotted in dimensionless form in figure 11, together with the theoretical curve of (2.44). The agreement is good although there is some degree of scatter, with

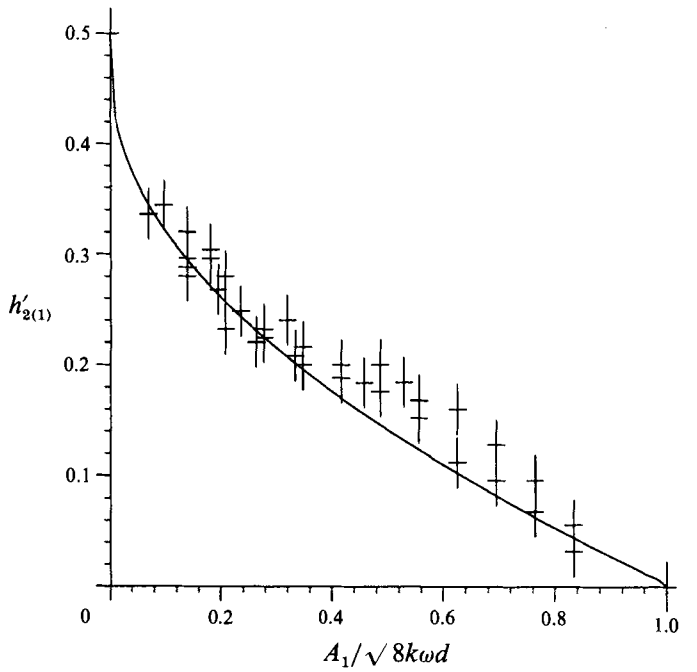


FIGURE 11. The variation of the secondary outflow height with vent area: comparison between the experimental data, and the theoretical curve of (2.44).

the large error bars reflecting the difficulty of measurement, particularly for vents of larger areas.

The mean value of $k$ measured using the above method was found to be $k = 0.51 \pm 0.03$. This is somewhat less than the value of $k = \sqrt{2}$ that would be expected (Linden *et al.* 1990) in the case of stationary buoyant fluid above an outflow vent. This may be attributed to the fact that the layer is moving and angled when flowing through the vent, so that the effective area is smaller.

### 4.4. *The effect of a vent in the primary cell*

The final set of experiments were carried out with two vents on each side of the source, in a symmetric arrangement with one of the vents on each side close to the source, and the other at some distance away. With this arrangement the effect of the large inflow of environmental fluid sucked in through the near vents could be calculated.

It was predicted in §2.2.3 that the outflow rate $Q_2$ would rise by a value of approximately $21Q_p/62$, where $Q_p$ is the volume flux sucked in through each vent: the changes in $u_2$, $u_1$ and $g'_2$ are given in (2.52), (2.53) and (2.50). From (2.38) it can be seen that the minimum value of area, $A_m$, required to vent all the outflow is given by

$$k(h_2 g'_2)^{\frac{1}{2}} A_m = Q_2. \tag{4.1}$$

It may be shown that (Barnett 1991) the increase in $A_m$ as a result of opening the vent in the primary cell is approximately given by (assuming that $Q_p \gg Q_0$)

$$A_{\text{increase}} = \frac{15 Q_p \omega^{\frac{1}{3}}}{2^{\frac{29}{6}} k Q_0^{\frac{1}{3}} g_0'^{\frac{1}{3}}}. \tag{4.2}$$

It is expected that $Q_p$ is proportional to the velocity of the impinging jet fluid flowing over the vent, and this in turn is expected to be proportional to the exit velocity

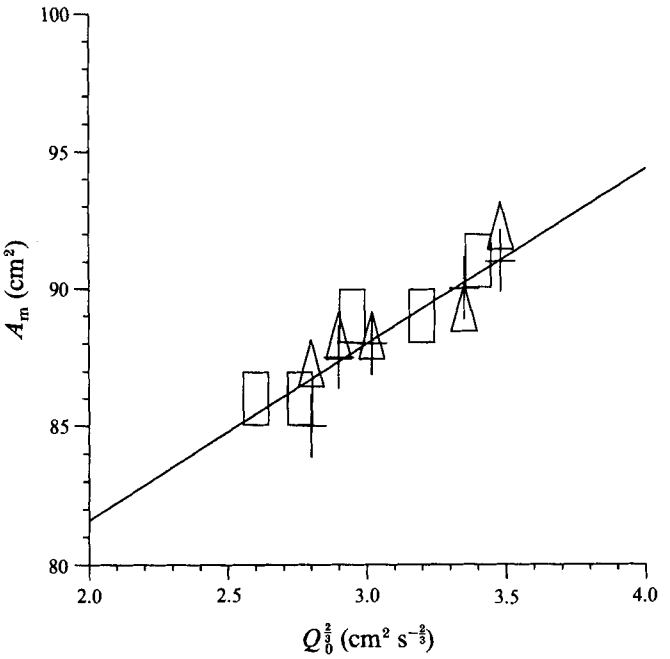


FIGURE 12. The variation of $A_m$ with $Q_0$. The different symbols denote measurements from three different experiments with the same source conditions.

of the source. Thus it is expected that $Q_p \sim Q_0$ and the increase in $A_m$ will vary as $A_{increase} \sim Q_0^{\frac{2}{3}}$.

Experiments were performed to test this result using a single vent either side of the source. The source flow rate was increased in intervals whilst keeping the area of the vents near to the source constant. A further vent at a large distance from the source was then opened to a large extent by sliding the base slats apart. The slats were then slowly closed until a point was reached at which further closure would mean that not all the buoyant layer was vented by that single vent. The area of the vent is then $A_m$.

The experimental data points for several experiments are plotted in figure 12, and exhibit the linear relationship between $A_{increase}$ and $Q_0^{\frac{2}{3}}$ described above. This comparison provides satisfactory evidence that the theory and assumptions of §2.2.3 are valid, although further experiments are required to test the dependence on the source velocity in equation (2.48), and to determine the nature of the function $f(x_p, g_c')$ (although the dependence on $x_p$ could be estimated by analysis of an impinging jet flow).

### 4.5. *Further experimental observations*

In addition to the experiments performed to make the measurements described above, some were carried out in a general investigation of other factors which may be of relevance in practical applications. Only brief descriptions are given here; for a more detailed account the reader is referred to Barnett (1991).

#### 4.5.1. *The effect of closing the ends of the tunnel*

In practical situations it is probable that the ends of the enclosing tunnel or duct will be closed. In experiments, closing the ends of the tunnel was observed to have negligible effect, except when (i) there were only a small number of vents, or (ii) the source was near to an end of the tunnel.

In the former case, there may not be sufficient vent area to vent the buoyant layer and also allow unrestricted flow into the tunnel from the environment. The buoyant layer may not then be fully vented before it reaches the ends of the tunnel, causing the buoyant layer to mix with the ambient layer at the tunnel end.

In the latter case there may be little or no ventilation between the source and the nearest closed end. The concentrations within this region and the primary cell will now reach higher values than before as now all of the buoyant fluid flows out in a single buoyant layer only.

4.5.2. *Asymmetric vent configurations*

Again, in practical situations it is unlikely that the vents will be symmetrically situated around the source. In experiments vent asymmetry was observed to be of little importance when all of the vents are outside the central mixed region: the positions of the vents in the counterflow has no effect on the central region and so the volume flux of the buoyant layer is the same on either side of the source. However, if there is a vent in the primary cell on one side of the source but not on the other, then there is an increased volume flux into the former side (due to the environmental fluid sucked in). Applying the model on each side of the source would imply a difference in the volume flux and concentration of the two buoyant layers. There was some evidence of this in the experiments as a larger number of vents were required to vent the buoyant layer on the side with the vent near to the source.

4.5.3. *Angled tunnels*

In this case, the high momentum of the source maintained the recirculating flow on both sides of the source but there was little further flow of buoyant fluid uphill, although fluid was still entrained into the primary cell on this side of the source. On the downhill side of the source there is a component of gravity acting to pull the buoyant fluid in the mixing region down the tunnel. This resulted in a breakdown in the counterflow system with fluid from the primary cell moving slowly down the tunnel, occupying nearly the entire depth. There appeared to be little entrainment on the downhill side of the source – all the entrainment took place on the uphill side.

## 5. Conclusions

The dynamics of a vertical, buoyant jet of high momentum in a long, possibly ventilated, tunnel have been investigated using a mathematical model and laboratory experiments. The analysis was developed assuming that the vents were symmetrically placed about the source, the ends of the tunnel were open and the jet length $L_j$ was several times the depth of the tunnel $d$, i.e. $\delta = L_j/d \gg 1$. The case of extremely large $\delta$, which results in the ambient fluid being flushed from the tunnel, has not been considered here.

The excellent agreement between the predictions of the theory and the experimental results indicates that the model gives a good description of the flow. For the main features of the model to be valid, it was found that $\delta \geqslant 2.9$ was required and so all the experiments were carried out under this condition. For all source values used within this range, the central mixed region near to the source had the same mean length of approximately $2.5d$. It must therefore be concluded that the effect of high source momentum in tanks of length $\lesssim 5d$ will be to mix the whole tank (provided that the source is vertical and centrally placed, that $\delta \geqslant 2.9$, and that the length of the tank is not too small).

Applying Benjamin's (1968) analysis of the flow over the 'head' of an air pocket in the present situation, it was deduced that the buoyant outflow should occupy half the depth of the tunnel $h_2 = \frac{1}{2}d$. This result was supported by almost all of the experiments, as are the consequent dependencies of the outflow velocity and reduced gravity on the source flow rate: $u_2 \sim Q_0^{\frac{1}{3}}$ and $g_2' \sim Q_0^{\frac{2}{3}}$. It should also be noted that the total volume flux of the outflowing buoyant fluid, $2Q_2$, is very much greater than that of the source; with the values suggested in §2.1.3, $2Q_2 > 33Q_0$, and hence a relatively small volume input will produce a much larger volume motion within the tunnel. The reduced gravity of the outflow is lower than that of the source by an equal factor. This solution (2.31)–(2.34) was used as the basis for the subsequent analysis of the flows over vents and the concentration build-up within the primary cell.

The time dependence of the central mixing region concentration was also calculated. In the analysis it was assumed that the volume flux of the buoyant outflow is dependent only on the mean concentration of the central region. The excellent agreement between the theory and experiment (figure 10) indicated the validity of this assumption. As suggested, it was found that the mean concentration of the central region, $g_c'$ is slightly higher than that of the outflow, $g_2'$ with $g_2'/g_c' = \kappa \approx 0.9$. Once the steady state is reached, which was within two minutes in all of the experiments, $g_2'$ appears to fluctuate by up to approximately 8% about its mean, maximum value.

The other aspect considered was the effect of ventilation points along the tunnel. There are four possible ventilation modes (which may occur in combination) depending on the position of the vent relative to the source.

Firstly, if all or part of the vent is within $\approx 2\alpha d$ of the source axis (where $\alpha \approx 0.1$), then the overlapping jet fluid will flow straight out of the vent. The jet fluid impinging between the vent and the source axis may still recirculate, but the flow system of figure 3 may not now apply. This situation has not been studied in any detail.

Secondly, if the vent is within the primary cell region, but is not sufficiently close to the source to allow the jet to flow straight out of the vent, then the pressure drop associated with the recirculating fluid causes environmental fluid to be 'sucked' into the recirculating cell. This results in an increase in the volume flux entering the primary cell and hence the volume flux of the buoyant outflow increases. The analysis showed that this increase in volume flux is about a third of the volume flux of the environmental fluid being sucked into the primary cell. The environmental fluid sucked in also acts to dilute the buoyant fluid, and so the concentration values are lowered.

Thirdly, if the vent is between the primary cell and the counterflow regions, then initially the recirculating fluid will suck environmental fluid through it as in the case above. However as the concentration of the central region increases to the steady state, the increasing buoyancy of the fluid above the vent increasingly opposes the weak inflow until the inflow is stopped and the buoyant fluid flows out.

Finally consider vents in the counterflow region. In §2.2.2 a simple analysis of the flow over a vent was developed. The importance of this analysis is that the volume flux and depth of any 'secondary' buoyant layer may be calculated. The analysis may then be applied repeatedly for successive outflow layers until all of the initial buoyant fluid layer has been vented. Thus this provides a method for calculating the total number of vents required to remove the buoyant outflow from the tunnel.

In §1, the flow caused by a leakage of a buoyant gas from a pipe in a duct or tunnel was given as one possible application of the model. Assuming that the density of the gas in the pipe was known, then, using the results presented here, it would be possible to calculate the minimum area required to vent the buoyant outflow created by a leak (see §4.4) using a single vent, assuming also that the leak was not so near to a vent so

that environmental fluid was sucked in. The spacing between the vents should be high so that the probability of the source being near to a vent is small, although if this were the case the maximum concentrations reached would be lower. Ideally, the ends of the tunnel should be open and if the ends are closed, the tunnel should extend some distance beyond the length of the gas pipe.

The author would like to acknowledge the advice of Dr P. F. Linden who has read several drafts of this paper without complaint. Dr R. P. Cleaver and Dr P. Cumbar have also made many valuable comments, particularly concerning a large-scale application of the model to the case of natural gas in air. The author also acknowledges the help of the DAMTP laboratory technicians, Mr D. Cheesely and Mr D. Lipman, with the experimental apparatus, and the invaluable assistance of Dr S. B. Dalziel with the use of the image processing.

Most of the work for this paper was carried out whilst the author was a PhD student in DAMTP, where his work was supported by the Science and Engineering Research Council and British Gas plc.

## REFERENCES

ANDREOPOULOS, J., PRATURI, A. & RODI, W. 1986 Experiments on vertical plane buoyant jets in shallow water. *J. Fluid Mech.* **168**, 305–336.

BAINES, W. D. & TURNER, J. S. 1969 Turbulent buoyant convection from a source in a confined region. *J. Fluid Mech.* **37**, 51–80.

BARNETT, S. J. 1991 The dynamics of buoyant releases in confined spaces. PhD thesis, University of Cambridge.

BENJAMIN, T. B. 1968 Gravity currents and related phenomena. *J. Fluid Mech.* **31**, 209–248.

ELLISON, T. H. & TURNER, J. S. 1959 Turbulent entrainment in stratified flows. *J. Fluid Mech.* **6**, 423–448.

JIRKA, G. H. & HARLEMAN, D. R. F. 1979 Stability and mixing of a vertical plane buoyant jet in confined depth. *J. Fluid Mech.* **94**, 275–304.

LEE, H.-W. 1980 Stability and mixing of a round buoyant discharge in shallow water. In *2nd Intl Symp. on Stratified Flows, Trondheim, Norway* (ed. T. Carstens & T. McClimans), pp. 881–897. Trondheim: Tapier.

LINDEN, P. F., LANE-SERFF, G. F. & SMEED, D. A. 1990 Emptying filling boxes: the fluid mechanics of natural ventilation. *J. Fluid Mech.* **212**, 309–335.

MONCRIEFF, M. W. & SO, D. W. K. 1989 A hydrodynamical theory of conservative bounded density currents. *J. Fluid Mech.* **198**, 177–197.

TURNER, J. S. 1973 *Buoyancy Effects in Fluids*. Cambridge University Press.

WILKINSON, D. L. & WOOD, I. R. 1971 A rapidly varied flow phenomenon in a two-layer flow. *J. Fluid Mech.* **47**, 241–256.